

Article

Significant Progress of Initiated Chemical Vapor Deposition in Manufacturing Soft Non-spherical Nanoparticles: Upgrading to the Condensed Droplet Polymerization Approach and Key Technological Aspects

Di Zhang ^{1,2} 

¹ Smith School of Chemical & Biomolecular Engineering, Cornell University, Ithaca, NY 14853, USA; dz283@cornell.edu

² Jilin Dongcheng Sumika Polymer Compounds Co., Ltd., Siping 136000, China

Abstract: Initiated chemical vapor deposition is a unique solvent-free and completely dry vapor-phase deposition technique used to synthesize organic polymer films. In this process, an activated initiator, monomer, and carrier gas are introduced into the reaction chamber simultaneously. This technique has been widely adopted. However, if the monomer and initiator are introduced into the chamber in stages—allowing gas-phase monomer deposition and condensation first, followed by initiator introduction and controlling the monomer partial pressure to be higher than the saturated vapor pressure—non-spherical polymer nanoparticles with dome-like shapes can be obtained. This advanced iCVD technique is referred to as the “Condensed Droplet Polymerization Approach”. This high monomer partial pressure gas-phase deposition is not suitable for forming uniformly composed iCVD films; but interestingly, it can rapidly obtain polymer nanodomains (PNDs). Using CDP technology, Franklin polymerized multifunctional nanodomains in less than 45 s, demonstrating a wide range of continuous particle size variations, from sub-20 nanometers to over 1 micron. This rapid synthesis included a variety of functional polymer nanodomains in just a matter of seconds to minutes. This review discusses the crucial process conditions of the Condensed Droplet Polymerization (CDP) Approach for synthesizing PNDs. The main focus of the discussion was on the two-step method for synthesizing PNDs, where the nucleation mechanism of PNDs, factors influencing their size, and the effect of pressure on the distinct condensation of monomer vapor into polymer nanodomains and polymer films were extensively explored.

Keywords: chemical vapor deposition; non-spherical polymer nanoparticles; condensed droplet polymerization



Citation: Zhang, D. Significant Progress of Initiated Chemical Vapor Deposition in Manufacturing Soft Non-spherical Nanoparticles: Upgrading to the Condensed Droplet Polymerization Approach and Key Technological Aspects.

ChemEngineering **2024**, *8*, 2.

<https://doi.org/10.3390/chemengineering8010002>

[chemengineering8010002](https://doi.org/10.3390/chemengineering8010002)

Academic Editor: Ewa Kowalska

Received: 21 August 2023

Revised: 12 October 2023

Accepted: 24 October 2023

Published: 19 December 2023



Copyright: © 2023 by the author. Licensee MDPI, Basel, Switzerland. This article is an open access article distributed under the terms and conditions of the Creative Commons Attribution (CC BY) license (<https://creativecommons.org/licenses/by/4.0/>).

1. Introduction

1.1. The Technical Background of CDP Synthesis Technique and the Significance of Synthesizing PNDs

Chemical vapor deposition (CVD) is a process in which the substrate is exposed to one or more volatile precursors that react and/or decompose on the substrate surface to create the desired thin film deposit [1]. Initiated chemical vapor deposition (iCVD) is a versatile technique that allows for solvent-free and completely dry vapor-phase deposition [2]. It offers numerous advantages, including the ability to achieve conformal and uniform fabrication over large surface areas. One of its key features is the real-time control it provides over the thickness and nanostructure of the deposited films [3]. In the field of nanomaterials synthesis, iCVD has garnered significant attention due to its superior capabilities in synthesizing various nanomaterials, including 1D, 2D, and 3D materials [4]. Specifically, in the realm of 1D materials, iCVD enables the fabrication of nanoparticles, nanowires, nanotubes, nanoribbons, and similar forms [5–7]. These materials possess

unique properties and find extensive applications in electronics, energy storage, sensors, and biomedical engineering [8–10].

The solvent-free and dry nature of iCVD allows for precise control over the composition and structure of the deposited polymer films, eliminating the need for post-deposition solvent removal steps and reducing the risk of contamination. Substantial research has emerged on the utilization of iCVD for polymer film applications on various substrates [11–14]. Notably, Karen K. Gleason and her team have made significant contributions in this area, particularly in the field of conformal polymer coating technologies. They have provided detailed insights into the synthesis process and system construction of polymer CVD [15–19].

The integration of iCVD synthesis with functional material design has fostered a burgeoning interdisciplinary field that combines materials science with microbiology [20,21]. This emerging field focuses on exploring the interactions between materials and microorganisms at the interface.

In the realm of biological applications, the design of materials with optimal biocompatibility and fouling resistance is of paramount importance. Biocompatibility refers to the ability of a material to interact with living systems without causing adverse reactions, while fouling resistance refers to the material's ability to prevent the accumulation of biological substances on its surface. Achieving optimal biocompatibility and fouling resistance necessitates a deep understanding of the complex interactions between materials and microorganisms, as well as precise control over material properties at the molecular level. Polymer nanodomains (PNDs) offer significant potential in drug delivery. They serve as effective drug carriers, safely encapsulating drug molecules within their sturdy polymer structures, protecting them from environmental factors such as humidity and light. PNDs can be tailored for controlled drug release, gradually delivering drugs to target tissues or cells by adjusting their size, shape, and polymer properties to meet specific therapeutic needs. Additionally, PNDs can be surface-modified for targeted drug delivery, adhering selectively to specific cells or tissues, enhancing drug precision while minimizing impact on healthy tissues. PNDs are typically biocompatible, causing minimal adverse reactions in biological systems, making them valuable for *in vivo* applications [22–26].

Polymeric nanoparticles can be synthesized using various techniques, such as emulsification (solvent displacement or diffusion) [27]. The latest technique for obtaining semi-spherical polymeric nanoparticles involves their polymerization through the method of initiated chemical vapor deposition [28].

In fact, current technology has advanced to the point where it is possible to synthesize nanoparticles on substrates with various shapes, such as nanodroplets, hemispheres, and domed shapes. The resulting deposit can encompass a range of materials including metals, semiconductors, alloys, and nanocomposites. The advanced iCVD polymers now have the capability of controlled anisotropy in the physical structure and chemical composition and are expected to pave the way for interface engineering toward innovative nanoparticle designs. Currently, polymer nanoparticles with a hemisphere (domed) shape, known as PNDs, are receiving significant research attention. This innovative nanoparticle design holds the potential to enhance drug delivery and improve the efficacy of precision medicine, showcasing remarkable attributes in drug delivery and biocompatibility. The size and shape of PNDs could potentially be critical factors influencing the stability and solubility of encapsulated cargo, facilitating membrane transport, and extending circulation time to enhance safety and efficacy in nanoparticle drug delivery systems.

1.2. Advantages of CDP Synthesis Technique for PNDs Formation Compared to Others

The traditional method for PNDs synthesis is emulsion polymerization, in which a low-water-soluble monomer is introduced into water along with a water-soluble initiator and surfactants. In these methods, stepwise polymerization occurs at the interface between two liquid phases, driven by the minimization of interfacial free energy, resulting in predominantly spherical PND shapes. However, the use of solvents poses several additional drawbacks, including limitations on the chemical functionalities achievable with solubilized

or emulsified monomers, the use of often toxic solvents or surfactants, and the need for costly additional purification steps to obtain a pure product (e.g., for nanomedicine). Furthermore, the requirement for purification extends the already time-consuming PNP synthesis protocols, which could take several days.

However, the CDP synthesis method introduces a novel approach that does not require the use of templates or solvents, similar to the iCVD (initiated chemical vapor deposition) technique. This method utilizes free radical polymerization to synthesize robust polymer nanodomains (PNDs) from vapor-phase reagents. In contrast to traditional methods, CDP does not rely on solvents or templates, thereby expanding the range of available shapes and chemical functionalities for PNDs. Moreover, CDP operates as a solvent-free system, eliminating the need for additional purification steps, enabling the rapid, one-step synthesis of high-purity PNDs, aligning with the principles of the iCVD technique.

Therefore, CDP technology offers advantages in PNDs synthesis over traditional techniques by being template-free, solvent-free, and reducing synthesis time. However, this technology has not been emphasized as extensively as it deserves.

1.3. Basic Steps of CDP Synthesis Process

The CDP preparation process can be summarized as follows: Initially, in a custom iCVD reactor, a fluorinated thin-film base layer was prepared on silicon (Si) wafers (Pure Wafer) using PFDA as the monomer. The silicon wafer was placed in the reactor chamber, which was maintained at a pressure of 400 mTorr, and a temperature-controlled stage kept at 35 °C. Subsequently, PFDA monomer vapor was delivered into the reactor chamber through a needle valve at a flow rate of 0.15 sccm, and argon carrier gas, as well as tert-butyl peroxide (TBPO), were introduced into the chamber through mass flow controllers at rates of 2.00 sccm and 0.60 sccm, respectively. A filament array was positioned approximately 3 cm above the substrate stage and heated to 300 °C to thermally decompose TBPO into tert-butoxyl and methyl radicals. These radicals initiated the thin-film polymerization upon contact with PFDA molecules adsorbed to the silicon wafer.

The subsequent step in CDP, which serves as the final phase, involves the rapid polymerization of liquid monomer droplets to solidify them into robust polymer nanodomains. To achieve this, TBPO was supplied to the reactor chamber at a rate of 1.8 sccm. Inside the chamber, the heated filament array at 300 °C decomposed TBPO into tert-butoxyl (TBO) and methyl radicals. These TBO and methyl radicals reacted with the nanoscale condensed droplets, initiating a free radical polymerization process that solidified the droplets into polymer nanodomains within a mere 45 s. Following this, the reactor chamber was evacuated and any unreacted materials were removed, resulting in high-purity PNDs, as shown in Figure 1.

In summary, the essence of the CDP method lies in controlling the formation of nanoscale, hemispherical condensed droplets and subsequently rapidly solidifying them into robust polymer nanodomains. This process is not dependent on the base layer material and can also be directly applied to the synthesis of PNDs on silicon substrates.

In Figure 1C, small blue circles represent precursors in the vapor phase. Precursor monomer flow is delivered to the deposition chamber. In Step 1 of CDP, nanoscale condensation is accomplished only by the introduction of monomers into the gas phase, whereas volatile initiators, such as tert-butyl peroxide, are not introduced. Monomers physisorb onto the substrate to be coated, and the filament above the reaction chamber is not enabled. The temperature of the substrate is kept at around 20–40 °C to promote monomer physisorption.

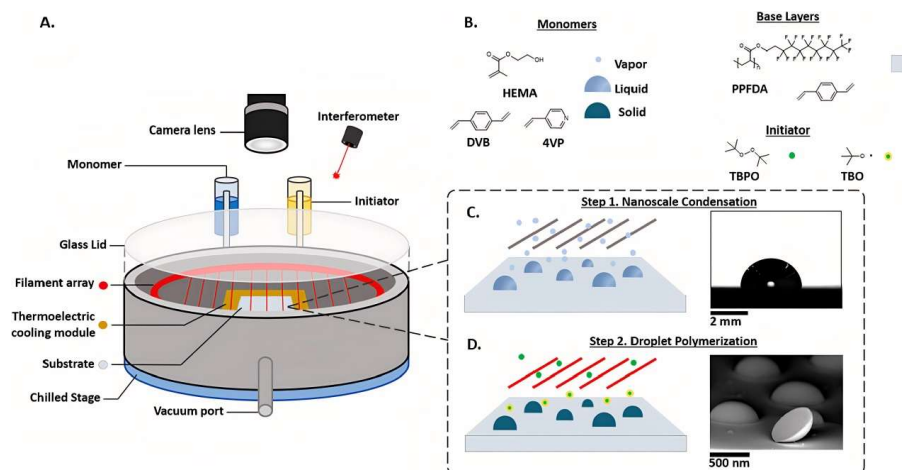


Figure 1. (A) depicts a schematic of the iCVD reactor, including a thermoelectric cooling (TEC) module for enhanced nanodrops formation and a digital microscope for real-time monitoring of the condensation-polymerization process. (B) illustrates the chemistry of the substrate surface, referred to as the “base layer,” and the polymerization initiator. (C) within the dashed box, the two steps of CDP are illustrated. In Step 1, vapor-phase monomers condense on the base layer placed on the TEC module, forming nanoscale droplets. (D) in Step 2, tert-butyl peroxide is delivered as vapor and undergoes thermal decomposition to tert-butoxyl (TBO) and methyl radicals, which occurs at a filament array maintained at 300 °C. These impinging free radicals initiate the polymerization and solidification of the condensed monomer droplets [29].

2. Condensation of Monomer Vapor into CDP: The Essential Requirement of Pressure above Saturation Vapor Pressure

Under conditions where the substrate temperature is lower than the ambient temperature and the surface energy is low, the condensation of water droplets can occur. Inspired by this phenomenon, Tao [30] first observed intriguing occurrences during the iCVD synthesis process when the pressure exceeded the monomer’s saturation vapor pressure. In such cases, the monomer vapor not only deposits on the substrate as a film but also undergoes gas-phase condensation to form droplets, which subsequently polymerize into non-spherical particles. However, achieving a pressure that surpasses the saturation vapor pressure is vital for the synthesis of PNPs (polymer nanoparticles).

In Figure 2, depositions were conducted on Teflon FEP-coated surfaces. In Figure 2d, the size of the polymer nanoparticles is around 5 μm , and the size of the PNPs increases with time. However, the shape of the polymer particles does not exhibit a uniform spherical crown morphology. On the other hand, from the image, it can be observed that during the nucleation stage, droplet coalescence occurs in the monomer condensation deposition process. Regarding the condensation of the monomer, it will be discussed later.

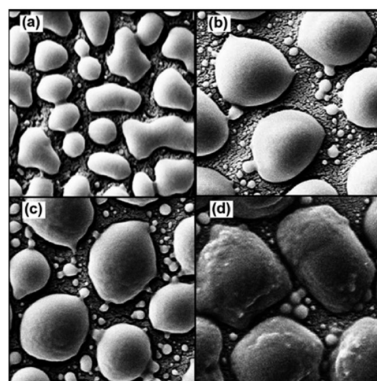


Figure 2. SEM images of poly(glycidyl methacrylate) nucleation ($P_m/P_{\text{sat}} = 1.45$) in iCVD; each figure is 5 $\mu\text{m} \times 5 \mu\text{m}$: (a) 5 min, (b) 10 min, (c) 15 min, and (d) 20 min [29].

Inspired by Tao, Franklin [30] also adjusted the P_m/P_{sat} ratio to be greater than one, resulting in PNPs instead of a polymer film. Monomer droplets were deposited on the surface of pPFDA. In the left image (at a 400 nm scale), taken during the first step of iCVD, the monomer vapor deposited and condensed to form PNDs that exhibited a noticeable hemispherical shape, as shown in Figure 3. This could be attributed to Franklin not directly depositing monomers on a silicon wafer substrate, but instead synthesizing a hydrophobic pPFDA film [31] first and then depositing the monomers, leading to polymer particles that were closer to a dome shape.

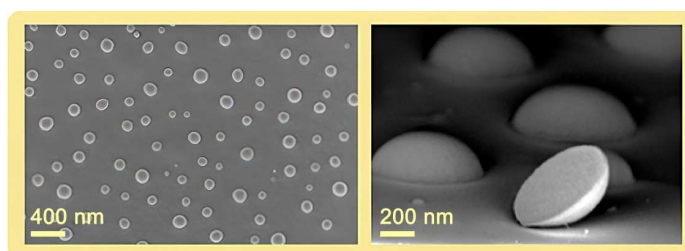


Figure 3. The SEM image of ndHEMA (2-hydroxyethyl methacrylate) nanodomains synthesized by the CDP technique shows the nanodome scale. A reactor chamber pressure of 300 mTorr; a filament array temperature of approximately 270 °C; and a stage temperature of 30 °C [29].

For depositions conducted beneath monomer saturation ($P_m/P_{sat} < 1$), smooth films were observed from the cross-sectional view of the polymer film ($P_m/P_{sat} = 0.72$) in Figure 4. Gupta [32] also mentioned that if the monomer pressure is kept below the saturation pressure, polymerization results in dense polymer films.

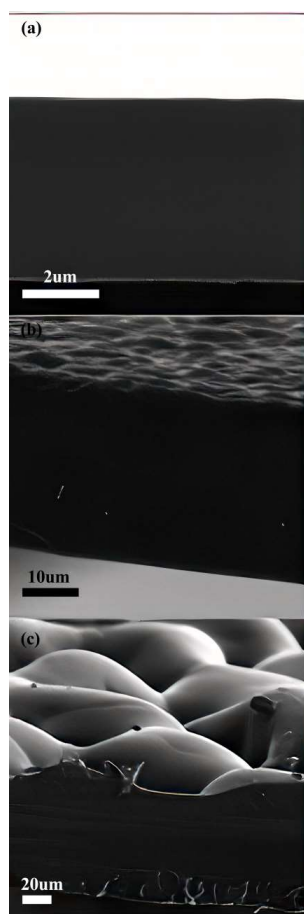


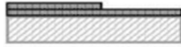
Figure 4. Cross-sectional SEM micrographs of vapor-deposited poly(glycidyl methacrylate) films: (a) $P_m/P_{sat} = 0.72$, (b) $P_m/P_{sat} = 0.99$, and (c) $P_m/P_{sat} = 1.45$ [30].

When monomer deposition occurs under gentle pressure conditions, the enhanced diffusion of monomers towards the substrate surface expands the spatial scope for aggregation or deposition. Decreasing monomer pressure reduces intermolecular interactions, facilitating improved control over film homogeneity and smoothness. Lower monomer partial pressure generally promotes a smoother, denser film morphology with diminished defects, owing to the prolonged surface diffusion time that allows the monomers to arrange into more orderly structures.

3. Three Designs of Vapor-Phase Monomer Deposition on Substrates in iCVD Process

D-growth refers to Droplet growth, which is the growth method designed based on the pressure ratio for deposition-type polymers. D-L growth, on the other hand, signifies a two-step growth mode of droplet condensation on the substrate of polymer film after formation. The growth process begins with the deposition of a polymer layer, followed by the subsequent Droplet growth on the polymer film. As shown in Table 1, both D-growth and D-L-growth occur when the partial pressure of the monomer is greater than the saturated vapor pressure. The difference lies in their choice of substrate. D-growth typically involves the direct synthesis of PNDs on a silicon substrate on the thermoelectric cooling (TEC) surface. On the other hand, D-L-growth involves synthesizing fluorinated polymeric films with a low surface energy, such as 1H,1H,2H,2H-perfluorodecyl methacrylate (PFDMA), 1H,1H,2H,2H-perfluorodecyl acrylate (PFDA) [32], and 1H,1H,2H,2H-perfluorooctyl acrylate (PFOA) [33] on the substrate before following the two-step method for PNDs synthesis in the same manner as D-growth.

Table 1. Polymer designed for deposition based on pressure ratio.

P_m/P_{sat} \ Design	Droplet Growth	Layer Growth	D-L Growth
$P_m/P_{sat} > 1$			
$P_m/P_{sat} < 1$			
$P_m/P_{sat} > 1$			

However, it is worth mentioning that Franklin subjected pPFDA to an annealing treatment to achieve a smoother layer for PNDs. The pPFDA films were placed in an oven set to 80 °C for 1 h. An annealing thermal treatment can enhance surface smoothness by eliminating organized crystalline domains responsible for surface protrusions. The polymerization monomers chosen for droplet growth can be HEMA (hydroxyethyl methacrylate), DVB (divinylbenzene), and 4VP (4-vinyl pyridine).

Layer growth refers to the one-step deposition of polymer solid-state films, accompanied by the simultaneous introduction of a decomposable initiator (TBPO), monomer, and carrier gas at specific flow rates.

Monitoring during the process of layer growth allows for in situ determination of the growth rate and for film growth to be terminated when a precise thickness is reached. High deposition rates (>1 $\mu\text{m}/\text{min}$) and film thicknesses (>200 μm) have been reported, as well as ultrathin pinhole-free CVD polymer layers (<10 nm).

4. The Intrinsic Mechanism for Forming Droplets Instead of Films

Greene [34] proposed that during the deposition process of vaporized water, there are two distinct ways in which atoms adhere based on their topological arrangement. One occurs at relatively high deposition rates ($P_m/P_{sat} > 1$), where the adsorbed atoms do not have enough time to diffuse to low-energy sites and are instead covered by subsequently deposited atoms, forming a pattern similar to that shown in Figure 5. This deposition growth mode can result in the formation of droplet-shaped polymer nanopar-

ticles and semi-spherical polymer nanoparticles, representing a non-continuous phase deposition pattern. This mode of growth is intriguing, resembling the mechanics of certain block-stacking games, where insufficient time for placement results in a continual upward stacking resembling triangular accumulation.

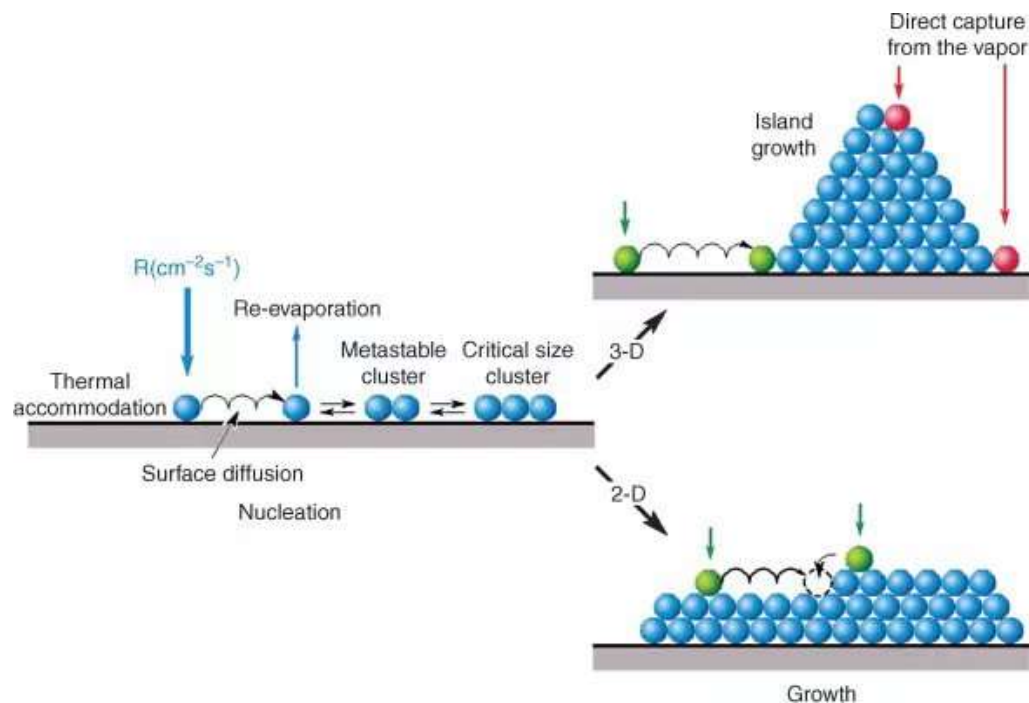


Figure 5. During the deposition process of vaporized water, island growth and layer growth modes [34].

The alternative mode of growth is a more gently inclined and even manner. In this scenario, the deposition rate is influenced by the partial pressure of the adsorbates. When the adsorbate partial pressure is lower than the saturation vapor pressure (i.e., $P_m/P_{\text{sat}} < 1$), the deposition rate becomes significantly lower, granting ample time for adsorbed atoms to settle into lower-energy sites, as illustrated by the adsorption sites in Figure 5. In this mode, as the deposition layer gets closer to the substrate below (with the substrate temperature lower than the ambient temperature), the temperature of the deposition layer gradually decreases. This leads to the stabilization of lower-energy sites, encouraging atoms to accumulate in a more uniform and consistent manner, resulting in the formation of a thin film.

These two distinct adsorption modes are dependent on the deposition rate and adsorbate partial pressure, influencing the diffusion and accumulation behavior of adsorbed atoms on the surface. This affects the formation of non-continuous phase structures like droplet-like or semi-spherical polymer particles, as well as thin films.

5. Two Steps: Condensation and Polymerization of Supersaturated Monomer Vapor

If the monomer deposition and polymerization are separated and carried out sequentially, the condition parameters during the monomer deposition process can be independently controlled, and it is also very beneficial for controlling the shape of the deposition, whether it is a polymer film or a polymer particle.

Table 2 shows a schematic of the sequential process for synthesizing porous polymers and nanodome polymers. Gupta's group [35,36] adopted a two-step approach to construct porous membranes composed of poly(methacrylic acid) (PMAA). Using this approach, Gupta's group [35,36] investigated membranes with porous morphologies, demonstrating the formation of pillar-like structures through substrate temperature variation during the monomer deposition step. Yang's group utilized the CDP synthesis route, where monomers such as HEMA, DVB, 4VP, etc., are condensed into droplets on the surface of a

hydrophobic polymer coating, followed by the introduction of an initiator to synthesize polymer nanodomains with a dome shape. Both groups share a common feature in which the initiator-initiated polymerization step is separated from the monomer deposition or condensation process, completing the synthesis in two steps. Despite leading to different polymer structures, they both employ a thermoelectric cooling device to effectively control monomer adsorption at the interface and substrate temperature.

Table 2. Comparison of two-step vapor-phase deposition: porous film generation process vs. nanodome formation process.

Steps	Schematic of Reactor	Similarity	Difference	Description
monomer vapor deposition into solid (1st)		thermoelectric cooling device (TEC)	when deposition, filament off	Porous Film deposition
polymerization (2nd)		monomer partial pressure influences the morphology of porous polymers and the deposition rate	in the first step, both monomers and initiators are introduced	
* after the two-step process, solid monomer sublimation				
monomer condensation into liquid (1st)		thermoelectric cooling device	when deposition, filament set on 300 °C	PNDs deposition
polymerization (2nd)		monomer partial pressure affects the size of domed polymers and the deposition rate	in the first step, only monomers are introduced	
* after the two-step process, unreacted monomer and initiator are removed by evaporation				

Moreover, in the first step of monomer deposition, the polymer morphology is influenced by the monomer partial pressure and deposition rate for both Gupta and Yang's groups. However, Gupta's two-step method slightly differs from the CDP process in PND synthesis. In the porous film generation process, during the first step when monomers are introduced into the reaction chamber, the initiator is also added; but, because the filament is turned off, the initiator does not decompose to generate free radicals, thus avoiding polymerization. The addition of the initiator in this step is intended to maintain the overall pressure of the reactor.

In contrast, the two-step method of the nanodome formation process does not introduce the initiator simultaneously with the monomers during the first step [37]. The filament remains active throughout, with only the monomer vapor adsorbing on the substrate surface, depositing, nucleating, growing, and coalescing. This process is akin to the condensation of liquid water droplets in mass transfer. Additionally, the design of the two-step process by the porous film generation process involves the first stage in which monomers are deposited and solidified at substrate temperatures of -20 , -10 , 0 , or 10 °C. The phase transition process involves the change from the gas phase to the solid phase.

On the other hand, the two-step method of nanodome formation process leverages the supercooling between environmental temperature and substrate temperature. Throughout the entire synthesis process, the filament is maintained at around 270 °C, resulting in high temperatures within the reaction chamber. However, the stage temperature remains around 30 °C. Under conditions where the pressure ratio is greater than one, monomer vapor on the

hydrophobic surface rapidly adsorbs, undergoes a gas–liquid phase transition, nucleates, grows, and coalesces into polymer droplets.

Following the polymerization reaction, both porous polymers and dome-like polymers contain residual unreacted monomers and initiators that necessitate removal from the reaction chamber to achieve the final solid state of the polymer. Despite occurring after the two-step synthesis, this stage is pivotal for achieving the ultimate morphology of PNDs or porous polymers.

Regarding PNDs, the elimination of unreacted constituents results in a substantial reduction in both the volume and aspect ratio, as discussed in Section 9. This observation underscores the presence of a notable amount of unreacted monomers and initiators during the polymerization phase. The porous film generation process indicates that due to the polymer formed at the vapor–solid interface acting as a diffusion barrier for free radical initiators, more than 90% of the monomer remains unused during the process of material removal.

The differentiation in the vapor–solid phase transition of the initial monomers introduces a slight divergence in the purging stage between the two synthesis methods. PNDs categorize this purging phase as “evaporation,” denoting the evaporation of unreacted monomers from the liquid phase. Conversely, porous polymers term this phase as “sublimating,” signifying the transition of unformed monomers from the solid phase to a gaseous state.

6. Variation of Droplet Radius with Surface Subcooling at Different Substrate Temperature

The most significant advantage of synthesizing polymer nanodomes based on iCVD, in addition to being solvent-free, template-free, having an in situ characterization, and being rapid, is the distinct separation of monomer deposition from the initiator-initiated monomer polymerization process. This enables clear observation of the size variations in the polymer nanodomes, facilitating precise control over the size of the nanodomes (PNDs).

During the first step of the two-stage control process, which involves the condensation phase of nanodomes, the filament within the chamber maintains the ambient temperature for monomer deposition throughout the chamber. However, as vapor-phase monomers come into contact with the bottom substrate, the nucleation, growth, and condensation of nanodomes are closely tied to the temperature of the substrate. The bottom substrate plays a crucial role in the gas–liquid interface phase transition.

James [37] focused his research on analyzing the impact of solid substrate temperature (T_s) during CDP on the growth of monomer droplets and the distribution of particle sizes. While keeping the monomer partial pressure constant, he examined how PNDs are influenced by variations in T_s .

Figure 6 depicts SEM images of the PNDs obtained on a pPFDA-coated substrate at temperatures of 21 °C, 24 °C, 27 °C, and 30 °C, with a scale bar of 200 nanometers [37]. From the comparison in the graph, it is evident that as the substrate temperature decreases, the final size of solidified nanodomes increases. This phenomenon is linked to the driving force behind particle nucleation. When a droplet reaches the minimum energy required for nucleation, it attains a critical radius to form a droplet nucleus. This concept draws parallels with the nucleation formula observed for water droplets under certain degrees of supercooling.

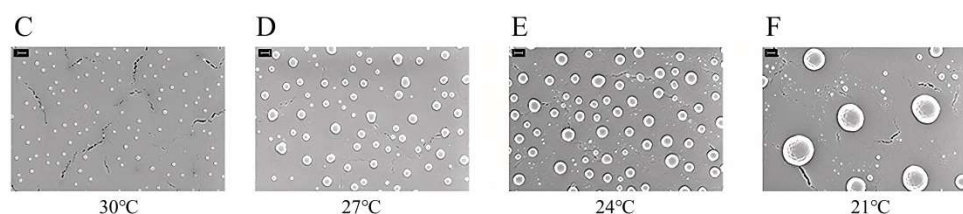


Figure 6. Size distributions of pHEMA PNDs obtained at substrate temperatures (T_s) of 21 °C, 24 °C, 27 °C, and 30 °C. Panels (C–F) show SEM images of the PNDs obtained at each T_s on a pPFDA-coated substrate, with a scale bar of 200 nm [38].

In iCVD, a Temperature-Controlled Stage (TEC) device [38] is typically installed at the bottom to regulate the substrate temperature. When the substrate temperature is lower

than the ambient temperature, it provides supercooling for the nucleation and growth of nanodomains. Investigating the size variation patterns of nanodomains at different degrees of supercooling is of significant interest.

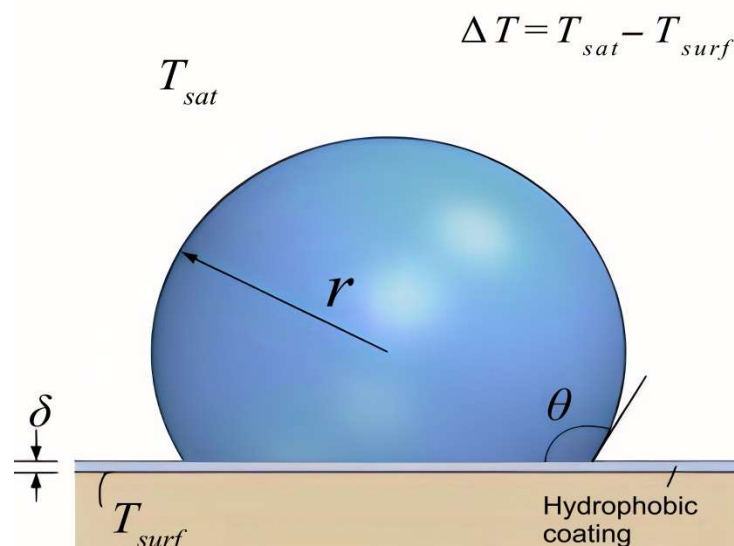


Figure 7. Nucleation of water droplets on hydrophobic surfaces and minimum critical radius [39].

The sub-cooling degree $\Delta T = T_{sat} - T_s$ is the difference between the saturation temperature of the water vapor T_{sat} and the surface temperature T_s , σ_l is the surface tension of the liquid, and H_{fg} and ρ_l are the latent heat of the liquid and the liquid density, respectively. The critical nucleation radius [40,41] is the minimum radius at which the nucleation droplet can keep thermodynamic stability, as shown in Figure 7. Once nucleation occurs on surfaces, continuous condensation on the droplet surface promotes the growth of droplets. Although this is a model for the mass transfer of water, it can be applied analogously to the nucleation of monomers in the liquid state. As the temperature, T_s , decreases, the temperature difference, ΔT , also decreases, resulting in an inversely proportional increase in the radius of the nucleation droplet.

7. Polymerization Time and Condensation Time

CVD (chemical vapor deposition) polymerization techniques not only demonstrate advantages in polymer thin film applications, but also for the synthesis of polymer particles. Gas-phase deposition helps circumvent the limitations of conventional solution-based PNPs (polymer nanoparticle) synthesis procedures. This is evident not only in terms of solvent-free conditions but also significantly reduces the required polymerization time. Franklin observes that the entire polymerization process of synthesizing nanodome particles through CVD can be completed in a matter of seconds. Moreover, in the experiment, after the condensation of monomer droplets, free radicals initiate the polymerization and solidification of nanodomains in less than 45 s.

This polymerization process is much faster than the time required for CVD technology to synthesize films, and James is also highly confident in this aspect. He took twice the amount of time compared to Franklin to ensure the complete polymerization of monomer droplets, and it only took 2 min. Therefore, a key step in the two-step synthesis of nanodomains, droplet-like, and cap-shaped polymer particles is the condensation phase.

During this phase, the monomers need sufficient time for nucleation to occur in liquid droplets with a critical radius, and the growth of these liquid droplets also requires time, including enough diffusion time for eventual coalescence, as shown in Figure 8 [41]. Considering the arrival of a single activated radical initiator into a condensed liquid monomer film, then about 1 s is required for the chain to grow to 104 g/mol. In dropwise

condensation, the process is cyclical, starting with the formation of liquid droplets at the atomic-scale selective nucleation sites. These droplets grow through stages of direct condensation, coalescence, and departure. This ensures a continuous cycle of condensation events. In the context of the CDP synthesis technique, the first phase involves the deposition of monomers on a solid surface, forming spherical liquid droplets. This process closely resembles the cyclical nature of dropwise condensation. Looking at the entire process, the condensation phase takes significantly more time compared to the second phase of the CDP synthesis, where monomers undergo polymerization initiated by radicals. Therefore, we can accurately say that the time scale for polymerization is a few orders of magnitude smaller than that of condensation.

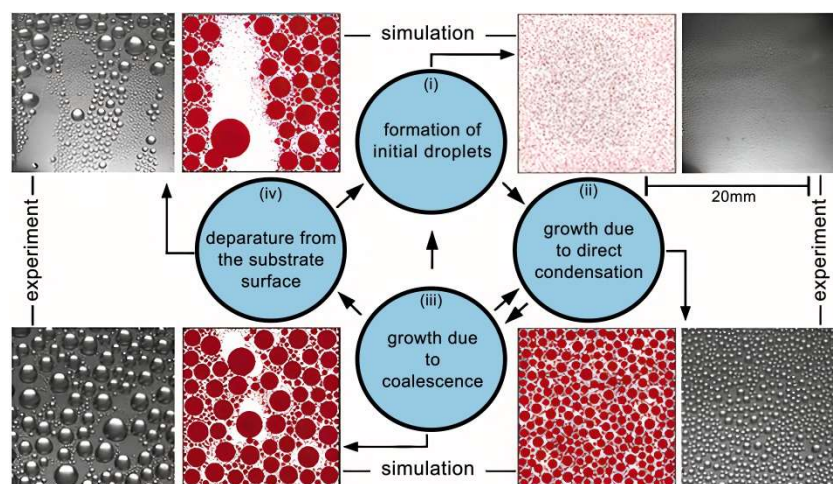


Figure 8. The cycle of major physical processes observed in the pendant mode of dropwise condensation on a horizontal substrate [41].

8. Size Reduction in Nanodomains in Two-Step Synthesis Due to Unreacted Initiator and Monomer Evaporation during Exhaust Process

The kinetic analysis indicates that the deposition process is constrained by adsorption, likely due to the limitation in the surface concentration of monomers. This result supports the hypothesis that polymerization takes place on the substrate rather than the growth of polymer chains in the gas phase, followed by deposition. This finding makes the described synthetic approach highly suitable for coating uneven substrates or substrates with high dimensional complexity. Therefore, in the two-step approach, initiating the deposition and condensation of monomers in the gas phase to form liquid nanodomains, followed by introducing initiator-laden nanodomains for a solid-phase polymerization reaction, is highly insightful. The practice is inspiring. In determining the final dimensions of PNDs, apart from the crucial condensation phase, the evaporation step for removing the unreacted initiator and monomer from the chamber also plays a pivotal role.

The Figure 9 portrays the condensation and polymerization of nanodomains, succeeded by an evaporation-based degassing phase. Our recent findings suggest that as the monomers and initiators are extracted, the nanodomains undergo a conspicuous volume contraction.

In Figure 10, through in situ monitoring of nanodomains' size, it was observed that during the evacuation phase, the most significant reduction in the PNDs' size occurred between 52 and 54 s. Solid-phase PNDs exhibited noticeable volume contraction, and the entire contraction process took place within the brief interval from 52 to 58 s. Beyond 58 s, extending to 90 s and 140 s, our findings suggest that there was no apparent contraction in the outline of the PNDs. This indicates that the evacuation phase was of short duration but was crucial in determining the final size of the PNDs desired in the experiment.

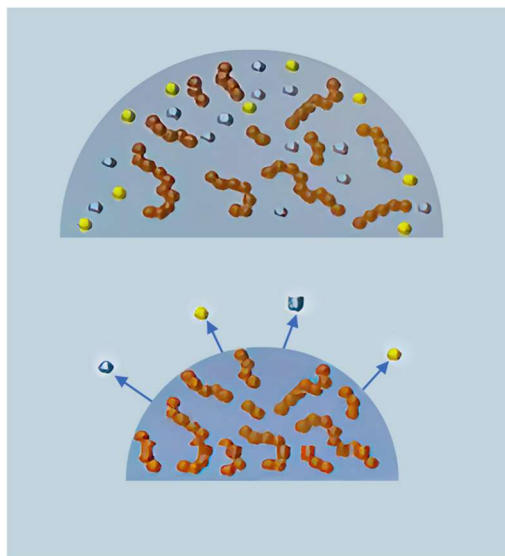


Figure 9. Extract unreacted monomers and initiators after polymerization. The yellow spheres in the diagram represent initiators, the blue spheres represent monomers, and the red spheres represent polymer chains.

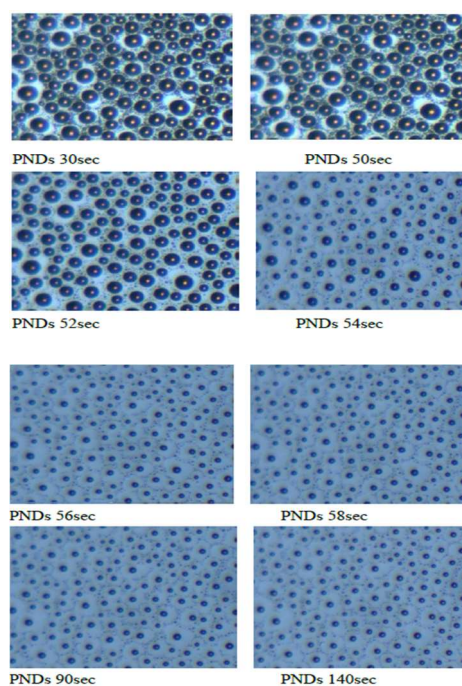


Figure 10. The evolution of PNDs' size over a duration of 2 min and 20 s during the stage of removing unreacted monomers and initiators, with a scale bar of 100 nm.

9. Discussion on Controllability Modeling of PNDs Particle Synthesis Using CDP Method

PNDs have the potential to enhance the stability and solubility of encapsulated cargo, facilitate membrane transport, and extend circulation times for increased safety and efficacy. Nanoparticle size and shape could be a significant factor influencing particulate drug delivery systems [42,43]. Hence, ensuring precise control over the nanoscale dimensions and aspect ratio of PNDs is of paramount significance. Tian and co-workers [44] fabricated cylindrical pore-shaped molds and then produced PDMS micro-pillar arrays through processes involving spin-coating, curing, and peeling. Utilizing initiated chemical vapor deposition (iCVD), they synthesized nanoscale pPFDA structures on the PDMS micro-pillar

arrays. This strategy of creating a micro/nanostructured PDMS-pPFDA superhydrophobic architecture offers valuable insights into the size control of PNDs.

As shown in Figure 11, after PDMS (poly(dimethylsiloxane)) was subjected to spin-coating, curing, and peeling off processes, it was placed onto the substrate inside the reaction chamber of iCVD. A single-step iCVD process was then utilized to synthesize the pPFDA film. The synthesis of pPFDA is not our primary focus; rather, it is the protruding micro-scale pillar arrays that we have identified as having the potential for the size-level control of PNDs. The presence of micro-structured PDMS constrains the dimensions of the pPFDA film to smaller levels. Consequently, this limitation extends to the size of the PNDs synthesized on the superhydrophobic pPFDA film. To achieve specific sizes for the PNDs, the employment of the protruding pillar arrays becomes advantageous. In a uniform protruding model, the process of nanodroplet coalescence on the nanodomains may be influenced. Smaller droplet nanodomains could potentially be lost due to the absence of neighboring nanodomains at the edges available for merging.

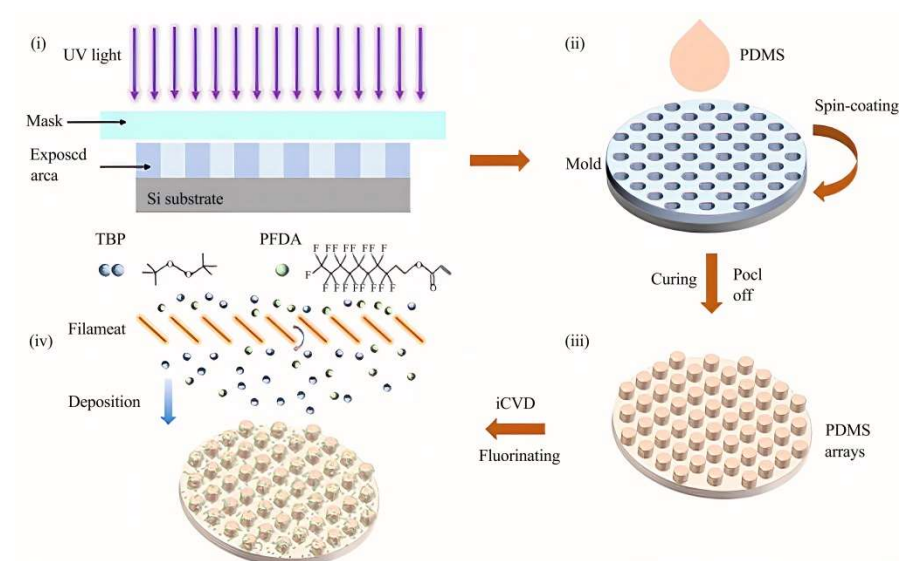


Figure 11. Schematic illustration of the strategy for superhydrophobic film preparation. (i) schematic of SU-8 molds (SU-8 photosensitive resin, a negative-tone, epoxy-based, near-UV photoresist, and they act as micro-nanostructure templates). (ii,iii) schematic of PDMS (poly(dimethylsiloxane)) arrays obtained by spin-coating, curing, and peeling off processes. (iv) schematic of the iCVD process [44].

10. Conclusions

This article primarily discusses the advantages, applications, and relevant parameters of an advanced initiation chemical vapor deposition (iCVD) process known as the chemical deposition polymerization (CDP) synthesis technique. The core principles of the CDP synthesis technique are twofold. Firstly, under conditions where the monomer vapor pressure is lower than the saturation vapor pressure, a hydrophobic polymer film with a smooth and uniform surface (such as pPFDA) is synthesized as the substrate. Secondly, a two-step method is employed to synthesize polymer nanodomains (PNDs). In the initial step, with the monomer vapor pressure higher than the saturation vapor pressure, the monomer vapor condenses, forming nanodome-shaped liquid droplets. In the subsequent step, by introducing an initiator and activating it using a filament, free radicals are generated. These free radicals then react with the previously formed nanodome liquid droplets, resulting in polymerization and solidification. The volume of the PNDs is significantly reduced due to the subsequent removal of unreacted monomers and initiators.

We primarily discussed an improved iCVD process, focusing on a novel route for synthesizing polymer nanoparticles—the chemical deposition polymerization (CDP) forming technique. We also summarized that the key aspects of this forming technique involve a two-step process (condensation followed by polymerization) and control of monomer vapor

p8pressure, which lead to the formation of drop-like or dome-shaped polymer nanodomains (PNDs). Furthermore, we compared and analyzed the two-step processes for porous polymer films and non-spherical polymer nanodomains. This comparison further confirmed the superiority of the two-step (condensation followed by polymerization) technique, which can inspire and influence the synthesis processes of various polymer forms using iCVD. This is particularly relevant in meeting the requirements for diverse polymers in areas such as biomedicine and drug delivery.

Funding: The author gratefully acknowledges funding support from the China Scholarship Council with post-doctoral fellow project. The funding number is 202108220128.

Data Availability Statement: Data openly available in a public repository.

Acknowledgments: I would like to express my gratitude to Rong Yang in the Smith School of Chemical and Biomolecular Engineering at Cornell University for providing me with the postdoctoral work environment and academic guidance.

Conflicts of Interest: Author Di Zhang was employed by the company Jilin Dongcheng Sumika Polymer Compounds Co., Ltd., the research was conducted in the absence of any commercial or financial relationships that could be construed as a potential conflict of interest.

References

1. Gleason, K.K. Nanoscale control by chemically vapour-deposited polymers. *Nat. Rev. Phys.* **2020**, *2*, 347–364. [[CrossRef](#)]
2. Gleason, K.K. (Ed.) *CVD Polymers: Fabrication of Organic Surfaces and Devices*; John Wiley & Sons: Hoboken, NJ, USA, 2015.
3. Alf, M.E.; Asatekin, A.; Barr, M.C.; Baxamusa, S.H.; Chelawat, H.; Ozaydin-Ince, G.; Petruczuk, C.D.; Sreenivasan, R.; Tenhaeff, W.E.; Trujillo, N.J.; et al. Chemical vapor deposition of conformal, functional, and responsive polymer films. *Adv. Mater.* **2010**, *22*, 1993–2027. [[CrossRef](#)] [[PubMed](#)]
4. Chai, Z.; Childress, A.; Busnaina, A.A. Directed assembly of nanomaterials for making nanoscale devices and structures: Mechanisms and applications. *ACS Nano* **2022**, *16*, 17641–17686. [[CrossRef](#)] [[PubMed](#)]
5. Song, Q.; Zhuang, L.; Fu, Q.G. Nanotube/nanowire-toughened carbon/carbon composites and their coatings. In *Nanomaterials in Rocket Propulsion Systems*; Elsevier: Amsterdam, The Netherlands, 2019; pp. 495–528.
6. Lazarus, L.L.; Riche, C.T.; Marin, B.C.; Gupta, M.; Malmstadt, N.; Brutchey, R.L. Two-phase microfluidic droplet flows of ionic liquids for the synthesis of gold and silver nanoparticles. *ACS Appl. Mater. Interfaces* **2012**, *4*, 3077–3083. [[CrossRef](#)] [[PubMed](#)]
7. de Melo Monteiro, A.P.; Dias Holtz, R.; Carneiro Fonseca, L.; Zanini Martins, C.H.; de Sousa, M.; de Luna, L.A.V.; de Sousa Maia, D.L.; Alves, O.L. Nano silver vanadate AgVO₃: Synthesis, new functionalities and applications. *Chem. Rec.* **2018**, *18*, 973–985. [[CrossRef](#)] [[PubMed](#)]
8. Azam, M.A.; Manaf, N.S.A.; Talib, E.; Bistamam, M.S.A. Aligned carbon nanotube from catalytic chemical vapor deposition technique for energy storage device: A review. *Ionics* **2013**, *19*, 1455–1476. [[CrossRef](#)]
9. Cai, Z.; Liu, B.; Zou, X.; Cheng, H.M. Chemical vapor deposition growth and applications of two-dimensional materials and their heterostructures. *Chem. Rev.* **2018**, *118*, 6091–6133. [[CrossRef](#)]
10. Ramachandran, R.; Mani, V.; Chen, S.-M.; Saraswathi, R.; Lou, B.-S. Recent trends in graphene based electrode materials for energy storage devices and sensors applications. *Int. J. Electrochem. Sci.* **2013**, *8*, 11680–11694. [[CrossRef](#)]
11. Ma, M.; Mao, Y.; Gupta, M.; Gleason, K.K.; Rutledge, G.C. Superhydrophobic fabrics produced by electrospinning and chemical vapor deposition. *Macromolecules* **2005**, *38*, 9742–9748. [[CrossRef](#)]
12. Tenhaeff, W.E.; Gleason, K.K. Initiated and oxidative chemical vapor deposition of polymeric thin films: ICVD and oCVD. *Adv. Funct. Mater.* **2008**, *18*, 979–992. [[CrossRef](#)]
13. Lau, K.S.S.; Gleason, K.K. Initiated chemical vapor deposition (iCVD) of poly (alkyl acrylates): An experimental study. *Macromolecules* **2006**, *39*, 3688–3694. [[CrossRef](#)]
14. Sojoudi, H.; McKinley, G.H.; Gleason, K.K. Linker-free grafting of fluorinated polymeric cross-linked network bilayers for durable reduction of ice adhesion. *Mater. Horiz.* **2015**, *2*, 91–99. [[CrossRef](#)]
15. Chen, N.; Kim, D.H.; Kovacic, P.; Sojoudi, H.; Wang, M.; Gleason, K.K. Polymer thin films and surface modification by chemical vapor deposition: Recent progress. *Annu. Rev. Chem. Biomol. Eng.* **2016**, *7*, 373–393. [[CrossRef](#)] [[PubMed](#)]
16. Zhou, Y.; Lachman, N.; Ghaffari, M.; Xu, H.; Bhattacharya, D.; Fattahi, P.; Abidian, M.R.; Wu, S.; Gleason, K.K.; Wardle, B.L.; et al. A high performance hybrid asymmetric supercapacitor via nano-scale morphology control of graphene, conducting polymer, and carbon nanotube electrodes. *J. Mater. Chem. A* **2014**, *2*, 9964–9969. [[CrossRef](#)]
17. Moni, P.; Al-Obeidi, A.; Gleason, K.K. Vapor deposition routes to conformal polymer thin films. *Beilstein, J. Nanotechnol.* **2017**, *8*, 723–735. [[CrossRef](#)]
18. Gleason, K.K. Overview of chemically vapor deposited (CVD) polymers. *CVD Polym. Fabr. Org. Surf. Devices* **2015**, *1*, 1–11.
19. Chan, K.; Gleason, K.K. A mechanistic study of initiated chemical vapor deposition of polymers: Analyses of deposition rate and molecular weight. *Macromolecules* **2006**, *39*, 3890–3894. [[CrossRef](#)]

20. Leonardi, A.K.; Ober, C.K. Polymer-based marine antifouling and fouling release surfaces: Strategies for synthesis and modification. *Annu. Rev. Chem. Biomol. Eng.* **2019**, *10*, 241–264. [[CrossRef](#)]
21. Chen, P.; Lang, J.; Franklin, T.; Yu, Z.; Yang, R. Reduced biofilm formation at the air–liquid–solid interface via introduction of surfactants. *ACS Biomater. Sci. Eng.* **2021**, *9*, 3923–3934. [[CrossRef](#)]
22. Zhou, H.; Bent, S.F. Fabrication of organic interfacial layers by molecular layer deposition: Present status and future opportunities. *J. Vac. Sci. Technol. A* **2013**, *31*, 040801. [[CrossRef](#)]
23. Yeo, L.P.; Yan, Y.H.; Lam, Y.C.; Chan-Park, M.B. Design of experiment for optimization of plasma-polymerized octafluorocyclobutane coating on very high aspect ratio silicon molds. *Langmuir* **2006**, *22*, 10196–10203. [[CrossRef](#)] [[PubMed](#)]
24. Montero, L.; Baxamusa, S.H.; Borros, S.; Gleason, K.K. Thin hydrogel films with nanoconfined surface reactivity by photoinitiated chemical vapor deposition. *Chem. Mater.* **2009**, *21*, 399–403. [[CrossRef](#)]
25. Zaporojtchenko, V.; Podschun, R.; Schürmann, U.; Kulkarni, A.; Faupel, F. Physico-chemical and antimicrobial properties of co-sputtered Ag–Au/PTFE nanocomposite coatings. *Nanotechnology* **2006**, *17*, 4904. [[CrossRef](#)]
26. Li, S.; Lin, M.M.; Toprak, M.S.; Kim, D.K.; Muhammed, M. Nanocomposites of polymer and inorganic nanoparticles for optical and magnetic applications. *Nano Rev.* **2010**, *1*, 5214. [[CrossRef](#)] [[PubMed](#)]
27. Mitchell, M.J.; Billingsley, M.M.; Haley, R.M.; Wechsler, M.E.; Peppas, N.A.; Langer, R. Engineering precision nanoparticles for drug delivery. *Nat. Rev. Drug Discov.* **2021**, *20*, 101–124. [[CrossRef](#)] [[PubMed](#)]
28. Sercombe, L.; Veerati, T.; Moheimani, F.; Wu, S.Y.; Sood, A.K.; Hua, S. Advances and challenges of liposome assisted drug delivery. *Front. Pharmacol.* **2015**, *6*, 286. [[CrossRef](#)]
29. Tao, R.; Anthamatten, M. Condensation and polymerization of supersaturated monomer vapor. *Langmuir* **2012**, *28*, 16580–16587. [[CrossRef](#)]
30. Franklin, T.; Streever, D.L.; Yang, R. Versatile and rapid synthesis of polymer nanodomains via template-and solvent-free condensed droplet polymerization. *Chem. Mater.* **2022**, *34*, 5960–5970. [[CrossRef](#)]
31. Lee, H.S.; Kim, H.; Lee, J.H.; Kwak, J.B. Fabrication of a conjugated fluoropolymer film using one-step iCVD process and its mechanical durability. *Coatings* **2019**, *9*, 430. [[CrossRef](#)]
32. Gupta, M.; Gleason, K.K. Initiated chemical vapor deposition of poly (1H, 1H, 2H, 2H-perfluorodecyl acrylate) thin films. *Langmuir* **2006**, *22*, 10047–10052. [[CrossRef](#)]
33. Oh, M.S.; Jeon, M.; Jeong, K.; Ryu, J.; Im, S.G. Synthesis of a stretchable but superhydrophobic polymer thin film with conformal coverage and optical transparency. *Chem. Mater.* **2021**, *33*, 1314–1320. [[CrossRef](#)]
34. Greene, J.E. Thin film nucleation, growth, and microstructural evolution: An atomic scale view. In *Handbook of Deposition Technologies for Films and Coatings*; William Andrew Publishing: Norwich, NY, USA, 2010; pp. 554–620.
35. Dianat, G.; Movsesian, N.; Gupta, M. Process–structure–property relationships for porous membranes formed by polymerization of solid monomer by a vapor-phase initiator. *Macromolecules* **2018**, *51*, 10297–10303. [[CrossRef](#)]
36. Dianat, G.; Movsesian, N.; Gupta, M. Vapor deposition of functional porous polymer membranes. *ACS Appl. Polym. Mater.* **2020**, *2*, 98–104. [[CrossRef](#)]
37. James, J.; Yang, R. Batch-Operated Condensed Droplet Polymerization to Understand the Effect of Temperature on the Size Distribution of Polymer Nanodomains. *Org. Mater.* **2023**, *5*, 148–157. [[CrossRef](#)]
38. Franklin, T.; Yang, R. Controlling Morphology of Polymer Particles Synthesized from Condensed Monomer Droplets. *Chem. Mater.* **2023**, *35*, 4955–4964. [[CrossRef](#)]
39. Leach, R.N.; Stevens, F.; Langford, S.C.; Dickinson, J.T. Dropwise condensation: Experiments and simulations of nucleation and growth of water drops in a cooling system. *Langmuir* **2006**, *22*, 8864–8872. [[CrossRef](#)]
40. Laaksonen, A.; Malila, J. An adsorption theory of heterogeneous nucleation of water vapour on nanoparticles. *Atmos. Chem. Phys.* **2016**, *16*, 135–143. [[CrossRef](#)]
41. Khandekar, S.; Muralidhar, K. *Drop Dynamics and Dropwise Condensation on Textured Surfaces*; Springer: Cham, Switzerland, 2020.
42. Haryadi, B.M.; Hafner, D.; Amin, I.; Schubel, R.; Jordan, R.; Winter, G.; Engert, J. Nonspherical nanoparticle shape stability is affected by complex manufacturing aspects: Its implications for drug delivery and targeting. *Adv. Healthc. Mater.* **2019**, *8*, 1900352. [[CrossRef](#)]
43. Marsh, B.M.; Iyer, K.; Cooks, R.G. Reaction Acceleration in Electrospray Droplets: Size, Distance, and Surfactant Effects. *J. Am. Soc. Mass Spectrom.* **2019**, *30*, 2022–2030. [[CrossRef](#)]
44. Tian, W.; Li, C.; Liu, K.; Ma, F.; Chu, K.; Tang, X.; Wang, Z.; Yue, S.; Qu, S. Fabrication of Transferable and Micro/Nanostructured Superhydrophobic Surfaces Using Demolding and iCVD Processes. *ACS Appl. Mater. Interfaces* **2022**, *15*, 2368–2375. [[CrossRef](#)]

Disclaimer/Publisher’s Note: The statements, opinions and data contained in all publications are solely those of the individual author(s) and contributor(s) and not of MDPI and/or the editor(s). MDPI and/or the editor(s) disclaim responsibility for any injury to people or property resulting from any ideas, methods, instructions or products referred to in the content.